Journal of Loss Prevention in the Process Industries 82 (2023) 104998

Contents lists available at ScienceDirect

Journal of Loss Prevention in the Process Industries

journal homepage: www.elsevier.com/locate/jlp

Performance-based assessment of an explosion prevention system for lithium-ion based energy storage system

Anil Kapahi [a,*], Alberto Alvarez-Rodriguez [a], Sunil Lakshmipathy [a], Stefan Kraft [a], Jens Conzen [a], Angelica Pivarunas [a], Rody Hardy [b], Paul Hayes [c]

[a] Jensen Hughes, Baltimore, MD, USA
[b] Powin, Tualatin, OR, 97062, USA
[c] American Fire Technologies, Wilmington, NC, 28405, USA

ARTICLE INFO

Keywords:
BESS
CFD
Explosions
Explosion prevention

ABSTRACT

This work developed and analyzed a design methodology for Powin Stack™ 360 enclosures to satisfy the requirements for explosion prevention per NFPA 855. Powin Stack™ 360 enclosures are lithium-ion-based stationary energy storage systems (ESS). The design methodology consists of identifying the hazard, developing failure scenarios, and providing mitigation measures to detect the battery gas and maintain its global concentration lower than 25% of the lower flammability limit (LFL) to meet the prescriptive performance criterion of NFPA 69 – Standard on Explosion Prevention Systems. The UL 9540A test data is used to define the battery gas composition, release rate, and release duration to describe the failure scenario involving thermal runaway propagation. The ESS enclosure consists of individual stacks (compartments) with targeted airflow to ensure the cooling of batteries during normal operational conditions. This arrangement makes it difficult to use a standard exhaust ventilation methodology to design an explosion prevention system. An innovative approach is used to purge the battery gas from individual Powin Stacks™ and from the main enclosure during a thermal runaway event. The designed method is analyzed using a computational fluid dynamics (CFD) model to ensure it meets the intent of NFPA 69. The explosion prevention system functionality presented in this work is limited to removing flammable battery gas generated due to the non-flaring decomposition of batteries and does not consider its interactions with other fire protection features.

1. Introduction

Energy storage is playing a pivotal role in empowering the decarbonization of transportation and enabling power grids to function with more resilience. Lithium-ion-based batteries have come a long way from their usage in consumer electronics with tens of Wh (watt-hour) capacity to approximately 100 kWh capacity battery systems in modern electric vehicles (Bisschop et al., 2020). Decarbonizing the electricity generation process is a big issue and critical to supporting the changing landscape in the automotive industry. Addressing this issue ensures we do not deal with greenhouse gases at the electricity generation source. Lithium-ion-based energy storage is one of the leading technologies for sustainable and emission-free energy. The advantage of storing green energy, such as solar or wind, during off-peak hours and using it during peak hours is gaining traction as various governments in the world look toward renewable energy sources. The growth in the energy capacity is tremendous, with the United States having less than 1 GW of large energy storage installations in 2019 to adding a capacity of 6 GW in 2021 and forecasted to achieve an additional 9 GW in 2022 (Blunt and Hiller, 2021).

Like many other energy sources, Lithium-ion-based batteries present some hazards related to fire, explosion, and toxic exposure risks (Gully et al., 2019). Although the battery technology can be operated safely and is continuously improving, the battery cells can undergo thermal runaway when they experience an exothermic reaction (Balakrishnan et al., 2006) of the internal cell components leading to a sudden release of thermal and electrochemical energy to the surroundings. These reactions cause thermal runaway occur when the internal separator of the anode and cathode is compromised due to some abuse of the cell (Ghiji et al., 2021; Roth et al., 2007) Cyclical thermal/electrical loading and unloading, manufacturing defects, and thermal, mechanical, or electrical abuse are many reasons that can cause cell degradation leading to

* Corresponding author.
E-mail address: akapahi@jensenhughes.com (A. Kapahi).

https://doi.org/10.1016/j.jlp.2023.104998
Received 30 June 2022; Received in revised form 20 December 2022; Accepted 24 January 2023
Available online 31 January 2023

thermal runaway (Bravo Diaz et al., 2020).

As the ESS enclosures are installed at an accelerating rate, a few incidents related to fires and explosions (Zalosh et al., 2021) have occurred. A detailed publicly available database on ESS failure events is maintained by the Electric Power Research Institute (EPRI) that provides a good overview of system capacity, age, event date, and its state during the accident (Long, 2022). The ESS community continues to learn from these incidents, and a lot of progress has been made to ensure the safety of these systems. NFPA 855 (NFPA, 2020) standard now requires ESS installation shall be provided with either an explosion control system, i.e., deflagration vents according to NFPA 68 (NFPA, 2018), or an explosion prevention system, i.e., a mechanical ventilation system according to NFPA 69 (NFPA, 2019). Essentially all ESS installations in the U.S. are required to have some form of explosion control unless the omission is demonstrated by large-scale testing. This paper focuses on developing a procedure to design an explosion prevention system for the Powin Stack™ 360 enclosure.

While the scope of NFPA 69 is extensive and applies to the design, installation, operation, maintenance, and testing of systems to prevent explosions using a variety of methods, this work is limited to the conceptual design of an explosion prevention system by pursuing the performance-based design option that aims at controlling the released battery gas combustible concentration. The system is designed using computational fluid dynamics (CFD) that helps in understanding the dispersion of battery gas within the enclosure. The usage of CFD for simulating an accidental release of flammable gas is well established. The CFD simulations can help demonstrate the evolution of gas release as a function of space and time.

Various metrics can be used to quantify the global parameters, such as volume fraction and mass within an enclosure. In addition, displaying the gas cloud between the lower flammability limit (LFL) and upper flammability limit (UFL) can help quantify the size of the flammable cloud. This detailed information is very useful in understanding the consequence of a scenario and designing the mitigation measures such as gas detection and explosion prevention systems.

The usage of CFD for designing explosion prevention systems is prevalent in process safety industries dealing with flammable fluids (Shen et al., 2020) and explosible dust (Eckhoff, 2009). Different scenarios involving spills, buoyancy-driven leaks, momentum-driven leaks, and a sudden loss of containment can be prescribed using a source term in the CFD model. These different leak scenarios require a deep understanding of the flammable fluid, storage and operating conditions, and the associated hazards. The critical challenge in designing an explosion prevention system for a ESS is to quantify the source term that can describe the release of battery gas during a thermal runaway event. The highly non-linear and stochastic behavior of battery cells requires a different approach from other failure scenarios commonly seen in the process safety industry, with greater emphasis on the availability of UL 9540A test (ANSI/CAN/UL, 2019) data to describe a battery gas release rate. In addition, the released battery gas is a mixture of hydrogen, carbon dioxide, carbon monoxide, and several hydrocarbons (Fernandes et al., 2018), requiring an approach to quantify mixture properties and flammability limits. Furthermore, the HVAC system used to cool the batteries can impact airflows with the formation of hot and cold aisles that can impact the placement of gas detectors as well as supply and exhaust locations for the explosion prevention system.

2. Design approach

2.1. Applicable standards

NFPA 855 (NFPA, 2020) requires that an explosion prevention system be installed in accordance with NFPA 69 (NFPA, 2019) for buildings and walk-in containers housing an ESS. NFPA 855 also indicates that a UL 9540A test or equivalent full-scale fire test shall be performed to evaluate the fire characteristics of an ESS that undergoes thermal runaway. NFPA 69 requires that the global combustible concentration shall be maintained at or below 25% of the LFL for all foreseeable variations in operating conditions and material loadings. The typical method to achieve this criterion is to use a ventilation/purge system that removes flammable battery gas from the container housing the ESS and replenishes it with outside clean air. For compliance with NFPA 855/NFPA 69 requirements to limit the flammable gas concentration, a representative release rate of battery gas during a thermal runaway scenario is required for the input to the explosion prevention analysis.

2.2. Design inputs related to the thermal runaway failure scenario

2.2.1. UL 9540A thermal runaway testing

NFPA 855 recommends that a UL 9540A (ANSI/CAN/UL, 2019) test be used to evaluate the fire characteristics of an ESS undergoing thermal runaway for explosion control safety systems. An approach to determine a flammable battery gas source term to design explosion control systems has been developed based on UL 9540A or similar test data. This approach aims to ensure that the process is consistent regardless of the battery system being evaluated. Information from the cell, module, and unit level UL 9540A test reports, or similar test data available, is used to calculate the composition, properties, amount, and duration of the flammable gas release.

The UL 9540A cell-level test defines a repeatable method for forcing a battery cell into thermal runaway. The standard requires measurements of the cell surface temperature as well as the temperature of the gas released from the cell during testing. Other important parameters used in the source term model include the gas volume released, gas composition, gas lower flammability limit, and the thermal runaway temperature of the cell which are measured as part of cell testing. (ANSI/CAN/UL, 2019). The reported thermal runaway temperature is the average of four tests. In a fifth cell test the gas volume and composition from the cell is measured. In separate testing, the previously measured composition of the gas is synthetically replicated and used to determine the LFL, burning velocity, and maximum explosion pressure.

The module- and unit-level UL 9540A tests are required if the cell vent gas composition is flammable according to ASTM E918 (2011). As over 90% of large scale ESS installations use lithium-ion batteries (U.S. Energy Information Administration, 2021), which contain flammable liquid electrolytes and release flammable gases during a thermal runaway event, module and unit level tests must be performed. One or more cells in the initiating module are forced into thermal runaway using the same or similar methodology used in the cell-level test. For the development of the source term, the extent and timing of thermal runaway propagation in the module and unit are used to construct an appropriate rate and duration of flammable gas release.

Additional conservatism may be added to the source term to account for the various types of uncertainty present in this analysis. This includes test-to-test variability, the thermal runaway initiation method, and conditions compared to an actual scenario, as well as general experimental uncertainty. For example, different thermal runaway initiation methods can yield more or less released gas from the cell (Essl et al., 2020). To add conservatism to the source term, the actual cell release volume and gas composition are used in combination with a shorter time to propagate thermal runaway. This method results in a higher overall average gas release rate than using the overall timing from the UL 9540A test.

2.2.2. Representative Powin Stack™ 360 ESS enclosure

A representative 53-ft Powin Stack™ 360 ESS enclosure was used for the CFD analysis. The overall dimensions of this enclosure are 53 feet long, 8 feet wide, and 9.5 feet high. This enclosure contains 14 Powin Stacks™ and a non-habitable control room at one of its ends. The two HVAC inlet ducts run the length of the container at the top, with ducting and cable racks present above the battery stacks. A cut section of the ESS enclosure provides details of the ESS interior in Fig. 1.

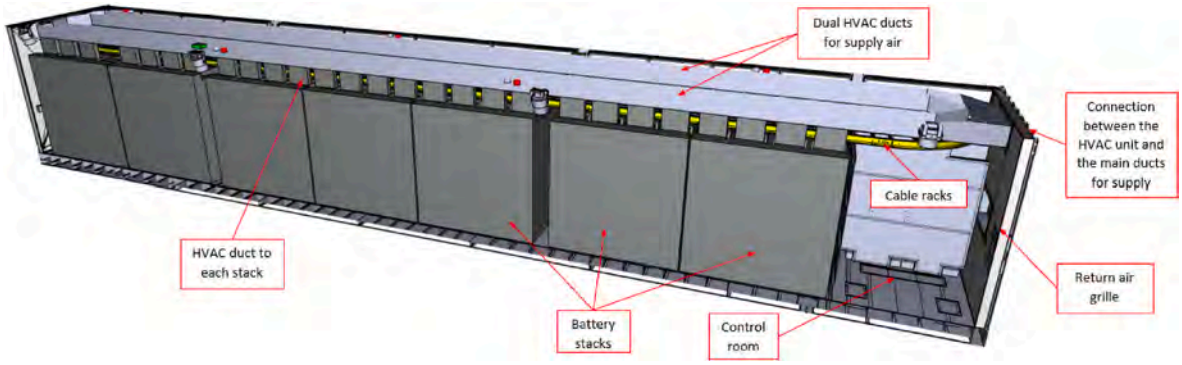

Fig. 1. Powin Stack™ 360 enclosure interior with battery stack layout and other internal equipment.

Each of the 14 Powin Stacks™ consists of 2 separate half stacks in their left and right cabinets, as illustrated in Fig. 2, housing the battery packs and the battery management system (BMS). There are 23 battery packs, with each battery pack consisting of 2 battery modules. The Powin Energy Stack 360 module consists of nine prismatic LFP cells. Each Powin Stack ™ has a total of 16 stack fans, 8 for each half of the stack, which provide airflow into the Powin Stacks™. These stack fans at the top are connected to the main HVAC supply duct of the ESS enclosure.

The airflow pattern within the battery stack is illustrated in Fig. 3. The total airflow rate is 800 CFM (0.38 m^3/s) from the eight stack fans for each half of the stack. Airflow to the stack fans is ducted from one of the two main HVAC supply ducts. Air exchange between the cold aisle and hot aisle is only through the battery module. As designed for this work, stack fans get activated by the BMS if a cell temperature goes higher than T_{th}[1] inside the battery module. Activation of the stack fans based on cell temperature would imply that the stack fans are operating at their full capacity prior to an accidental battery gas release. These fans are then assumed to be running before the cells undergo thermal runaway and are assumed to be running throughout the battery gas release duration. This HVAC configuration is noted as "HVAC ON" in this work.

2.2.3. *Powin Stack™ 360 ESS enclosure HVAC system*

The ESS container is equipped with two external self-contained wall-mounted HVAC units located on both ends of the container (see one HVAC unit connection illustrated in Fig. 1). Depending on indoor/outdoor environmental conditions, the HVAC units can function as.

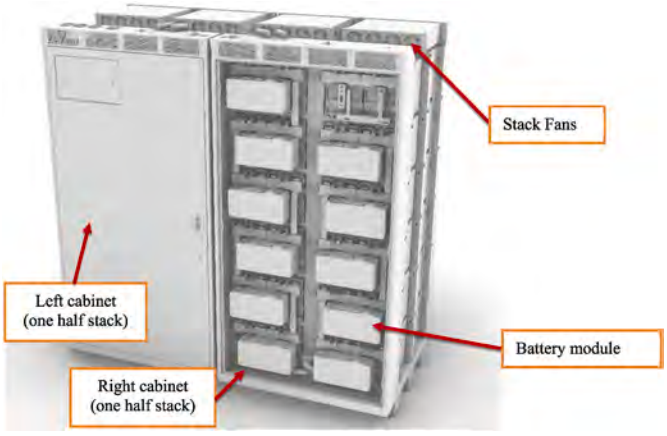

Fig. 2. Powin Stack™ 360 geometry.

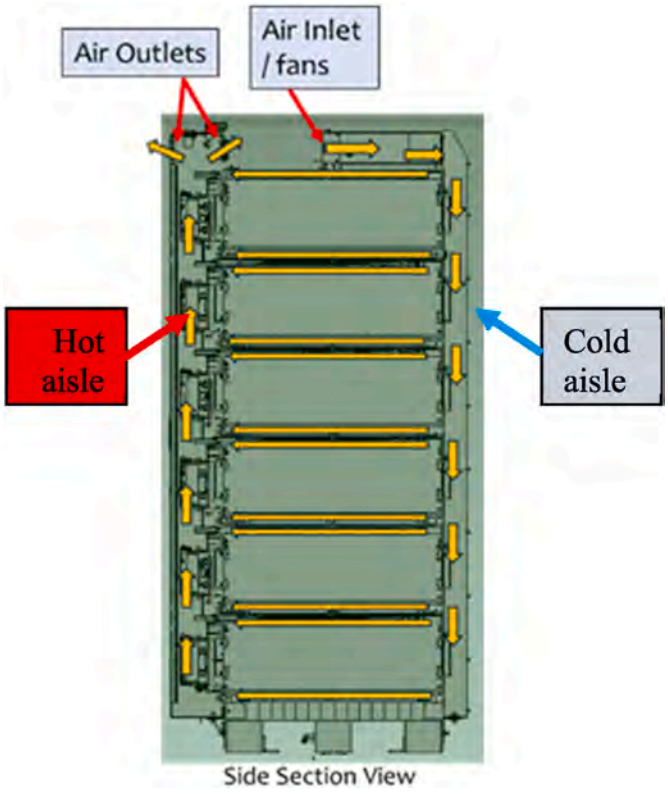

Fig. 3. Airflow pattern within the stack.

a) a 100-percent recirculation mode: no outside air is introduced in the enclosure while the air already inside is conditioned, or
b) a 100-percent economizer mode: outside air is conditioned and supplied into the enclosure, and an equivalent amount of inside air is exhausted to the exterior.

A diagram of these two HVAC modes (Marvair, n.d.) is shown in Fig. 4. Fig. 5 illustrates the air coming from the main ducts is connected to both HVAC units, enters via stack fans, and sweeps through each of the 14 stacks (batteries not shown) before getting out of the stacks by outlets located at the top.

2.2.4. *Powin Stack™ 360 ESS enclosure explosion prevention system*

Fig. 6 illustrates the components of the battery gas explosion prevention system of the Powin Stack™ 360 ESS container. Battery gas

[1] T_{th} is a threshold temperature much lower than the thermal runaway temperature.

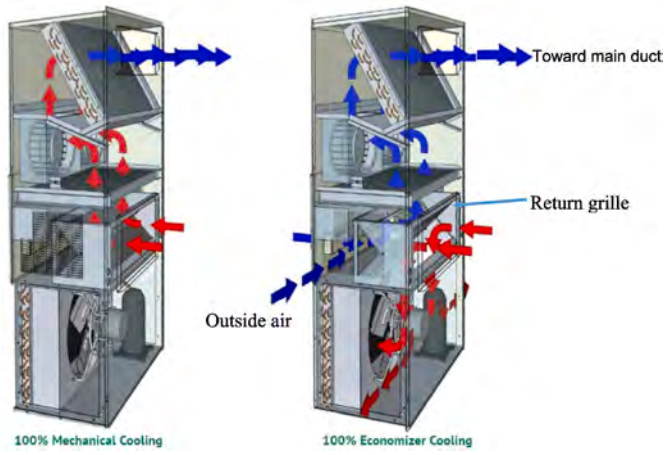

Fig. 4. Ventilation modes of the HVAC system.

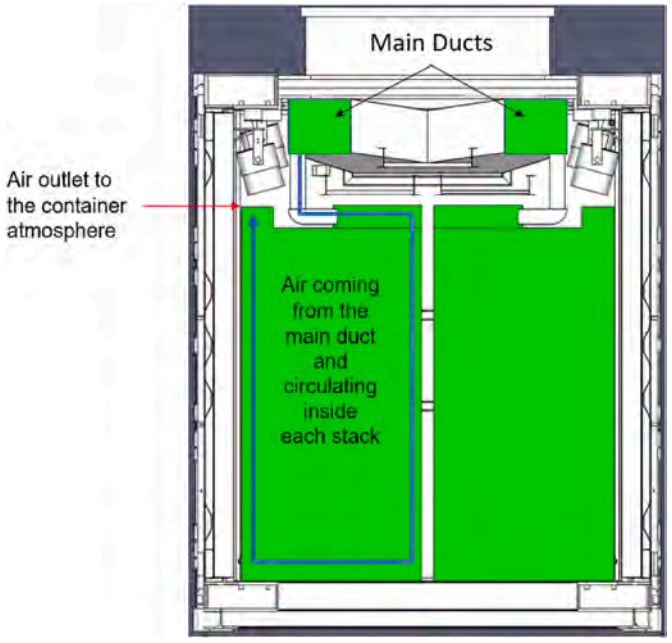

Fig. 5. Air transfer between one of the 14 stacks and the BESS enclosure atmosphere.

released during a thermal runaway event would be detected by one of the two hydrogen detectors located on the upper part of the container as shown in Fig. 6. After the hydrogen concentration (volume fraction) at one of the detectors reaches 0.1% (or 2.5% H_2 LFL), the activation of the explosion prevention system is assumed in this work to have a response time of 90 s. It should be noted that the explosion prevention system corresponds to the HVAC system in economizer mode. Fresh air at 3800 CFM (1.79 m^3/s) flowing through the dual HVAC longitudinal duct will sweep through the stacks before entering the main enclosure; this increased amount of the air inside the enclosure will cause the enclosure atmosphere containing battery gas to be exhausted outside via the two HVAC unit return grilles. In addition, the BMS ensures the 1600 CFM (0.76 m^3/s) (800 CFM (0.38 m^3/s) to each half) is directed to the stack with a cell temperature higher than the T_{th}, and the rest of the 2200 CFM (1.04 m^3/s) is distributed among the remaining stacks.

2.2.5. *Flammable battery gas release model*

Most UL 9540A data commissioned by manufacturers is proprietary. For this work, a set of representative thermal runaway data for a lithium iron phosphate ($LiFePO_4$) chemistry battery cell was used to develop the input flammable gas model for the CFD model. Based on the cell-level test, the battery gas composition is found to be as reported in Table 1. This battery gas is released at a temperature of 640 °C. The LFL of the battery gas was estimated for this work to be 6.14% based on testing the representative gas mixture at ambient conditions. The "safe" threshold considered in the analysis presented in this work is 25% of this LFL or 1.54%.

The module-level test is used to quantify the release rate of battery gas. Table 2 summarizes the characteristics of the two failure events considered in this work.

1. A single-module failure scenario is developed using the UL 9540A test data associated with a battery gas release of 1.65 g/s.
2. A two-module failure scenario is associated with a source term of 2.0 g/s.

The battery gas release rate scenarios were based on an analysis of UL 9540A test data using the approach outlined in Section 2.2.1. The scenarios were selected based on elevated temperatures (higher than the thermal runaway temperature) in cells in the modules. The timing of thermal runaway within a single module is based on an approximation of the realistic minimum propagation delay from observations during the testing.

Table 1
Battery gas composition from prismatic cell based on UL9540A test data.

Species	Vol. Percent
Hydrogen	48.69%
Carbon Dioxide	28.70%
Carbon Monoxide	9.86%
Hydrocarbons[a]	12.75%

[a] Hydrocarbons are assimilated to propane in the following CFD sections.

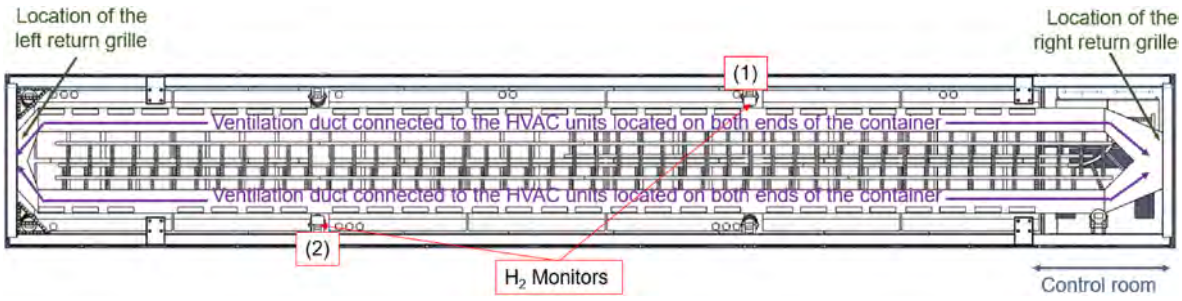

Fig. 6. Enclosure showing hydrogen detector location and HVAC exhaust locations.

Table 2
Characteristics of the Powin Stack™ 360 ESS container failure events.

Event Description	Number of Cells involved	Failure Mode	Average gas release rate (g/s)	Total duration (min.)	Assumptions
Single-module failure	9	Cell overheating or power surge affecting one module	1.65	14.5	Propagation to all cells in one module in series (five cells) & parallel (two cells in a thermal runaway at one time)
Two-module failure	18	Cell overheating or power surge affecting two modules	2.0	24	Propagation to the second module occurs at 550 s (half the median time to 200 °C in the module level tests)

2.3. Design tool

The design tool used in this work is a CFD model called Fire Dynamics Simulator (FDS) (McGrattan et al., August 21). FDS is a computer fire model developed by the National Institute of Standards & Technology (NIST). For the type of analysis performed in the work, using a series of conservation equations for mass, momentum, and energy transfer, FDS can evaluate over time the dispersion of the battery gas based on the different release scenarios while predicting the time when the detectors would actuate and activate the explosion prevention system, simultaneously deactivating the HVAC cooling system.

Documentation of the model, including validation studies, is readily available (McGrattan et al., NIST Special Publication 1019, sixth edition (FDS Version 6.7.5), August 21, 2020). FDS version 6.7.5 was used for the present work.

2.4. Approach for the CFD analyses

A two-step approach is adopted for this work to understand the dispersion and accumulation of battery gas inside the failing stack and the ESS enclosure. The first step (enclosure-level analysis) involves understanding the accumulation of battery gas inside the main enclosure, assuming all of the battery gas released inside a failing stack is directly released into the enclosure atmosphere, which is a conservative hypothesis for the dispersion of battery gas inside the enclosure, as some of the released battery gas may remain inside the failing stack. The second step (stack-level analysis) is to understand the accumulation of battery gas inside an individual stack, assuming some of the battery gas released into the enclosure would eventually re-enter the stack while the HVAC unit operates in the recirculation mode.

Table 3
Simulation Timeline of both CFD Dispersion Analyses.

Event	Event Time (s)
Start of the HVAC system in recirculation mode	−30 s
Start of battery gas release	0
H_2 detection threshold is reached at one of the two H_2 detectors	t_1
Activation of the explosion prevention system	$t_1 + 90$ s
The explosion prevention system reaches its full capacity after a linear ramp of 20 s	$t_1 + 110$ s
Battery gas release stops	t_2 seconds

Both CFD analyses use the same simulation timeline (Table 3) in which the battery gas disperses in the container and is detected by one of the two hydrogen detectors, and the hydrogen detection results in the activation of the explosion prevention system. In Table 3, (t_1) is estimated during the enclosure-level dispersion analysis, and (t_2) corresponds to the end of the battery release as indicated in Table 2 for the two selected failure scenario events.

3. Modeling methodology

This section provides an overall modeling methodology for the two corresponding levels of CFD analysis: the enclosure dispersion analysis and the internal Stack 360 dispersion analysis.

3.1. Modeling setup for the enclosure dispersion analysis

The CFD model illustrated in Fig. 7 is based on the 3D CAD geometry of the enclosure imported in the software PyroSim developed by Thunderhead Engineering. This model was augmented with point devices to monitor the hydrogen concentration with time. In addition, the HVAC module of FDS was used to set up the HVAC cooling supply and return nodes. At this point, the container had all of its physical features captured that can be used for the CFD analysis. The enclosure material was assumed to be stainless steel of thickness 3 mm. The contents of the enclosure are also assumed to be stainless steel of thickness 3 mm with insulated backing, i.e., no heat loss to the backside boundary.

Each FDS computational cell was a cube of 0.125 feet or 1.5 inches to capture enough detail without a prohibitive computational time. The computational domain was divided into approximately 40 meshes.

Free volume calculations were performed to quantify the amount of space where battery gas can accumulate inside the enclosure. These calculations were performed by assuming all of the obstructions within the enclosure to be solid, including the stacks and the HVAC duct. In that case, the enclosure atmosphere's free volume was 27.3 m^3 (964 ft^3). The dispersion of the battery gas inside the stack with the failing battery is the subject of the internal dispersion analysis detailed in Section 3.2 of this article.

3.2. Modeling setup for the internal stack dispersion analysis

The CFD geometry of the half stack with the battery gas release location indicating the failed module is shown in Fig. 8. A 1-cm uniform mesh size was chosen to balance the computational time against resolving the gaps in the battery modules to capture the airflow patterns inside the stack with the failing battery. The resulting free air volume is estimated to be 0.51 m^3 (18.01 ft^3).

4. Modeling results

This section describes the results of the two CFD dispersion analyses used to design the explosion prevention system.

4.1. Powin Stack™ 360 global dispersion analysis results

4.1.1. Battery gas concentration within the enclosure atmosphere

In this scenario, the battery gas would disperse via entrainment by the HVAC system flow. For each of the two selected failure scenarios, a two-step simulation strategy was used to analyze the different failure scenarios with the HVAC system ON configuration.

Step 1. A CFD simulation was performed to evaluate H_2 detection times. These times were evaluated to occur at 44 s after the start of the single-module failure scenario and at 37 s after the start of the two-module failure scenario,

Step 2. A CFD simulation was then performed, with the activation of

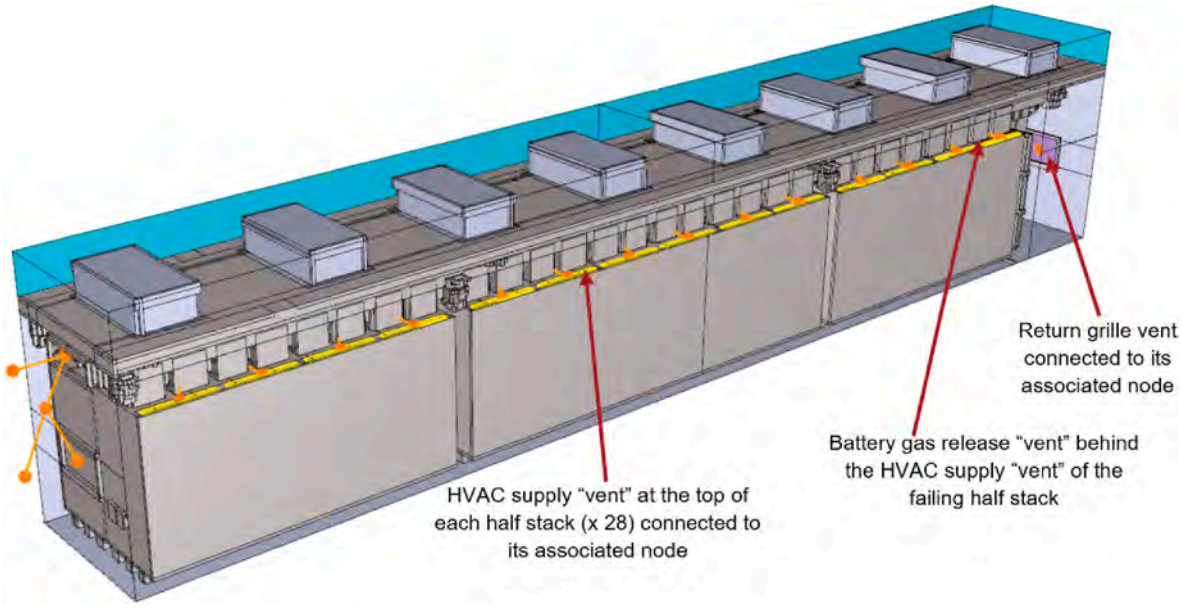

Fig. 7. FDS HVAC components of the Powin Stack™ 360 enclosure.

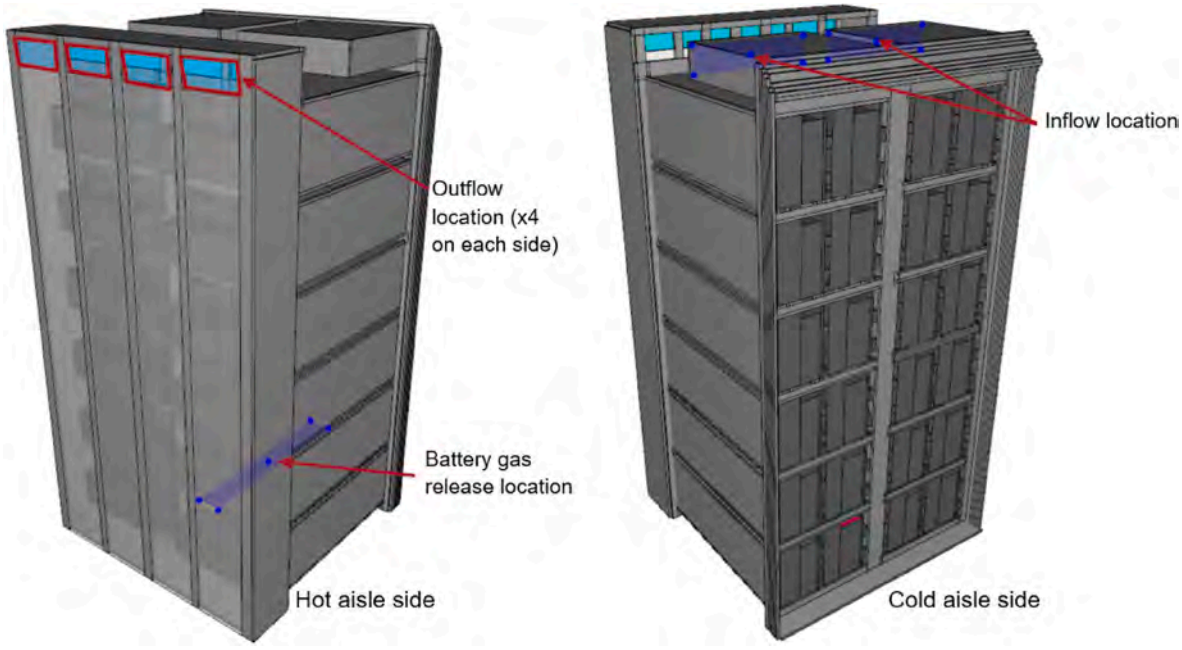

Fig. 8. *Inflow and outflow vent configuration in the CFD geometry for the internal stack dispersion analysis.*

the explosion prevention system 90 s after the detection times estimated in Step 1 increased by a safety factor of 20%.

Fig. 9 shows the global battery gas volume fraction for the two failure scenarios (Step 2), with the maximum estimated at 1.09% or 17.8% LFL for the single-module failure scenario and 0.94% or 15.4% LFL for the two-module failure scenario. These results indicate that the global battery gas volume fraction would remain below the threshold criterion of 25% LFL.

Fig. 9 also shows that before the activation of the ventilation system, the time evolution of the battery gas volume fraction is linear, as the battery release is constant and occurs within an enclosed domain with 100% recirculation.

After detection, the battery gas volume fraction decreases as the explosion prevention system discharges some of the battery gas outside the container. As long as the battery gas release continues, there is an equilibrium between this source of battery gas and its depletion by the explosion prevention system. When the battery release ends, the battery gas concentration within the ESS enclosure generally falls to zero within a minute for the two considered failure scenarios.

Fig. 10 illustrates the evolutions of the battery gas mass in the container over time for the CFD analysis failure scenarios. These evolutions follow the same trend as the battery gas global volume fraction, as illustrated in Fig. 9.

The evolution of battery gas dispersion from its release location to the adjacent control room and the rest of the enclosure is shown in Fig. 11 for various times of the two-module failure scenario. The battery gas volume fraction immediately decreases well below 25% of its LFL after the activation of the explosion prevention system, as shown in

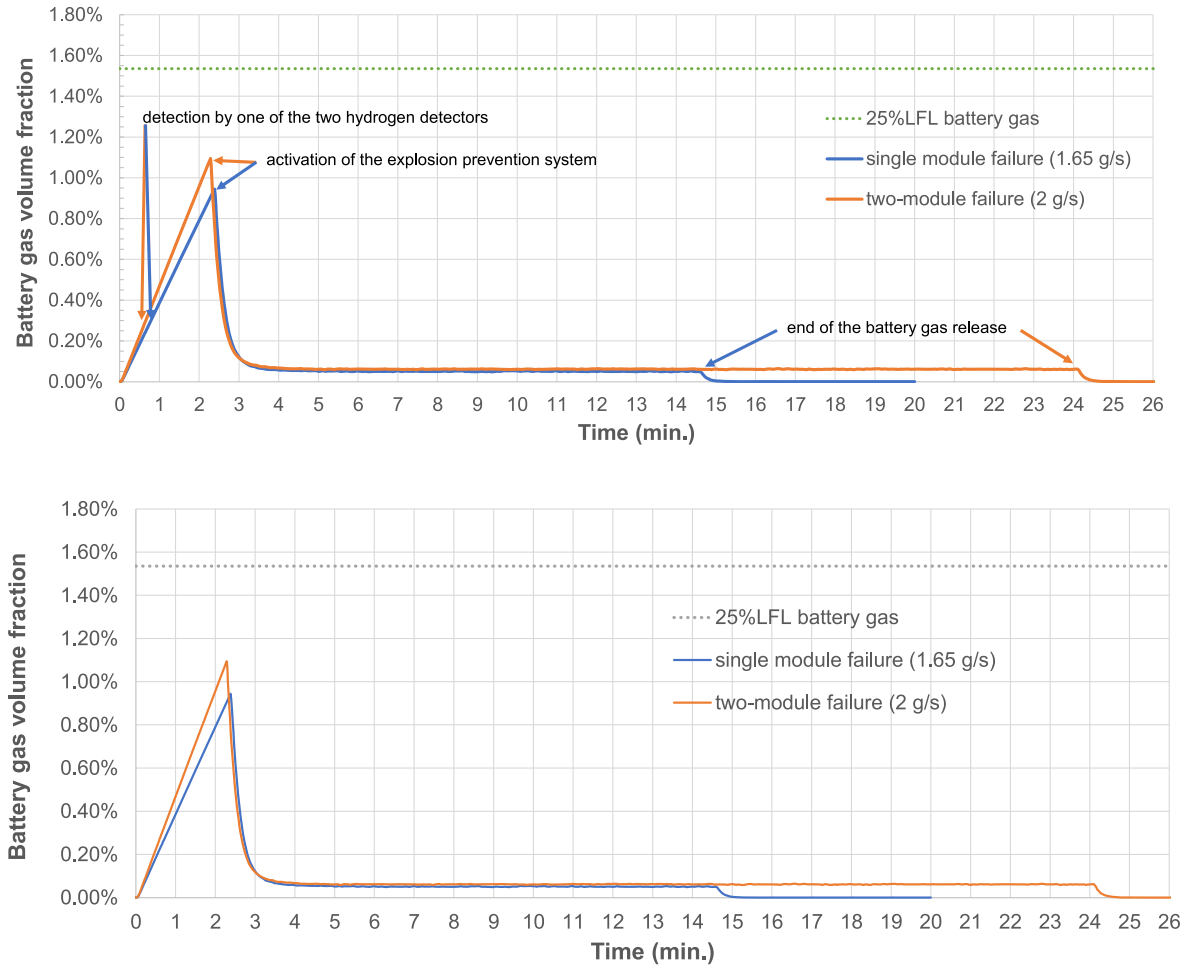

Fig. 9. Evolutions over time of the global battery gas volume fraction for the two considered failure events.

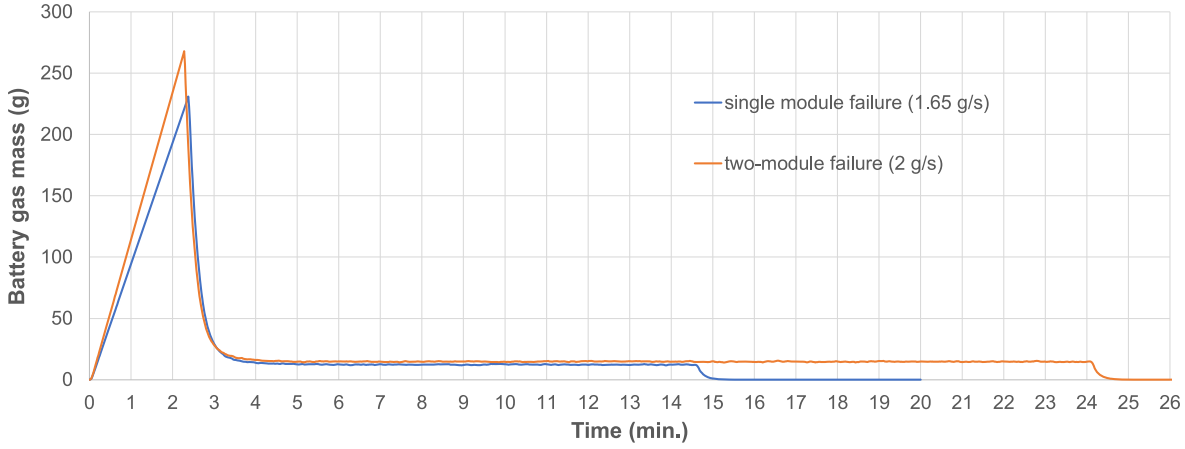

Fig. 10. Evolutions over time of the global battery gas mass for the two considered failure events.

Fig. 11 at 3 min. Note that the local concentrations at the release location can be higher than LFL.

4.1.2. Estimation of the recirculating air contamination with battery gas

The CFD simulations at the enclosure level were also used to determine the contamination of the recirculating air as it flows through the HVAC system. The battery gas contaminates the recirculating air before the explosion prevention system is activated. Based on the CFD model illustrated in Fig. 7, it is possible to estimate the battery gas mass flow rate re-injected into the failing half stack as a portion of the recirculating air increasingly becomes contaminated by battery gas before activation of the explosion prevention system.

Fig. 12 shows that before the activation of the explosion prevention system, the battery gas mass flow that is re-injected into the failing half stack increases to approximately 5 g/s for the single-module failure event and 5.8 g/s for the two-module failure event. This result can be explained by the fact that the failing half stack is located near the control room, where battery gas tends to accumulate, as illustrated in Fig. 11. A

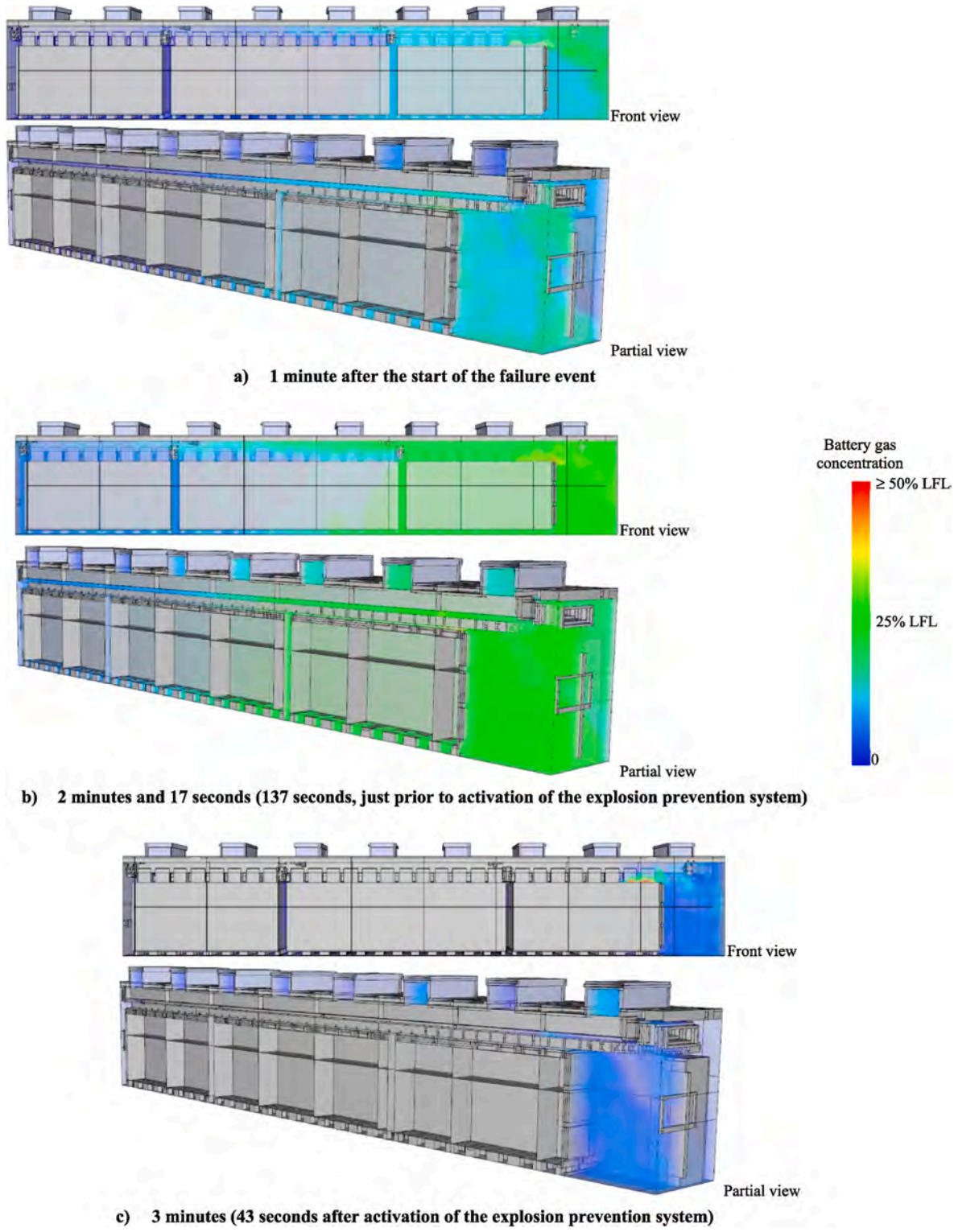

Fig. 11. Battery gas 3D profiles for the two-module failure event.

total of 800 CFM (0.38 m^3/s) or approximately 450 g/s of contaminated air passes through the failing half stack. The CFD simulations showed that the battery gas volume fraction at the right HVAC return grille would increase to approximately 1.7% (26.6% LFL), corresponding to a battery gas mass fraction of 1.3%. A simple calculation of the battery gas returning to the failing half stack based on the total mass flow and battery fraction (450 × 0.013 = 5.85 g/s) at the right return grille validates the results presented in Fig. 12. Note that the other 13 stacks would also encounter the air contaminated with battery gas entering through the stack fans during the recirculation mode. But it is crucial to quantify the battery gas entering through stack fans for the failing stack, as this will augment the total amount of battery gas that can accumulate inside the stack. This information is used as an input for the stack-level analysis, presented in the next section.

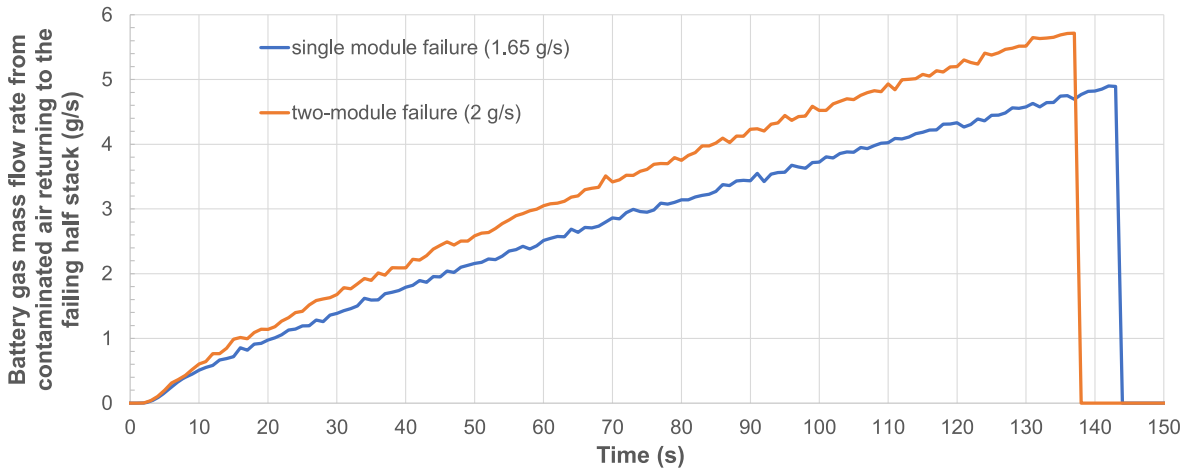

Fig. 12. Rates of battery gas returning to the failing half stack for the two considered failure scenarios.

4.2. Internal stack 360 dispersion analysis results

CFD analysis of the Powin Stack™ 360 internal dispersion analysis is performed by considering the battery gas release to occur from a module close to the bottom of the half stack, which is a conservative assumption since the resulting released battery gas would have to disperse through the height of the stack to be ejected outside the stack into the enclosure atmosphere. Variation of the battery gas mass inside the failing half stack cabinet is plotted in Fig. 13. The global battery gas concentration variation within the half stack cabinet is plotted in Fig. 14. The battery gas global statistics within the half stack increase until the explosion prevention system is activated, and clean air is then sent to the stack instead of the recirculating container air, which was becoming contaminated by battery gas, as shown in Fig. 12.

The residual mass of the battery gas within the stack increases up to 8.1 g for the single-module failure event and 9.75 g for the two-module failure event. These values drop to approximately 2 g after the explosion prevention system has been activated. The global concentration of the battery gas inside the failing half stack cabinet is above the 25% LFL limit for less than 1 min before the explosion prevention system is activated for both failure scenarios. The battery gas global concentration drops to 8% LFL during the steady operation of the explosion prevention system. Stack fans being active throughout the release of the battery gas ensure the global concentration within the stack cabinet remains low.

Contours of the battery gas vapor cloud colored by concentration are shown in Fig. 15 for the two considered failure scenarios just before the explosion prevention system is activated. The figure shows the battery gas vapor cloud contours at the following locations.

- on the cold aisle side through which the inflow air is directed,
- on the hot aisle side from where the battery gas is exhausted out of the stack, and
- from a side-view between the stacked battery packs.

Fig. 16 shows the total battery gas emission (source and inlet) compared to the total battery gas exhausted for the half stack for a single-module failure scenario. The same information is provided in Fig. 17 for the two-module failure scenario. These figures indicate that the stack-level dispersion study is compatible with the container-level study presented in the previous section of this report. A low accumulation of battery gas in the failing half stack (Fig. 13) would marginally lower the mass flow rate at the exhaust points and will lead to.

- increase in the detection time for the hydrogen detectors in the container atmosphere (already considered at a 20% higher value for the container level),
- decrease in the global battery gas volume fraction inside the container (leading to a conservative container dispersion level study).

5. Conclusion

A CFD study was performed for the Powin 53-ft ESS enclosure to assess the capability of the explosion prevention system to maintain the

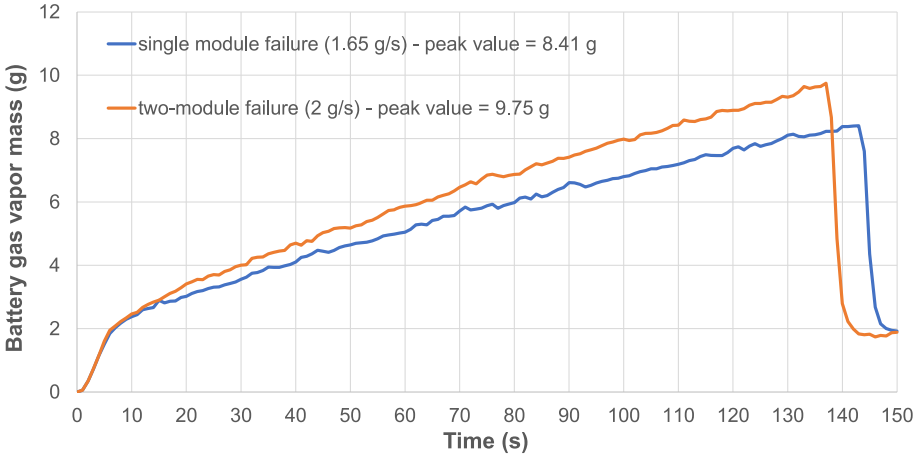

Fig. 13. Variation of battery gas mass inside the failing half Stack 360 cabinet.

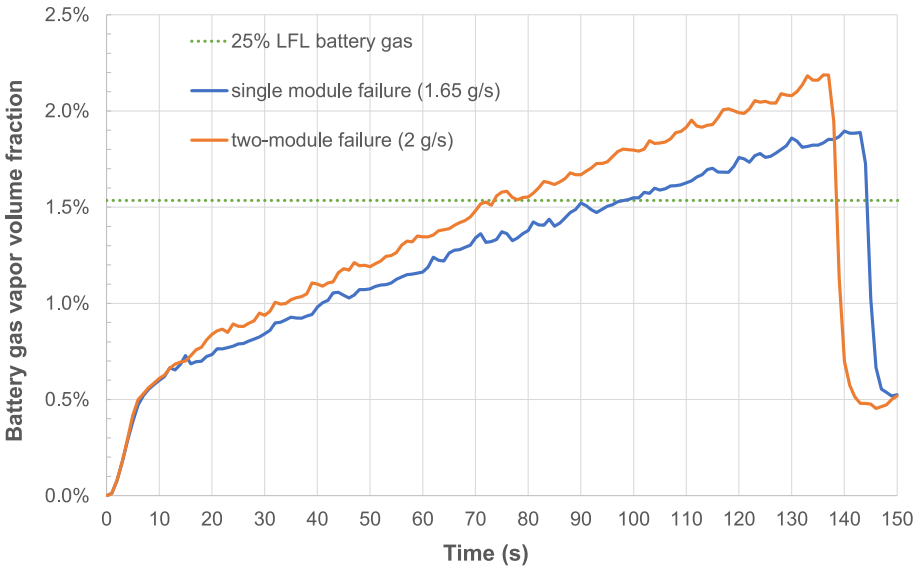

Fig. 14. Variation of battery gas global concentration inside the failing half Powin Stack™ 360 cabinet.

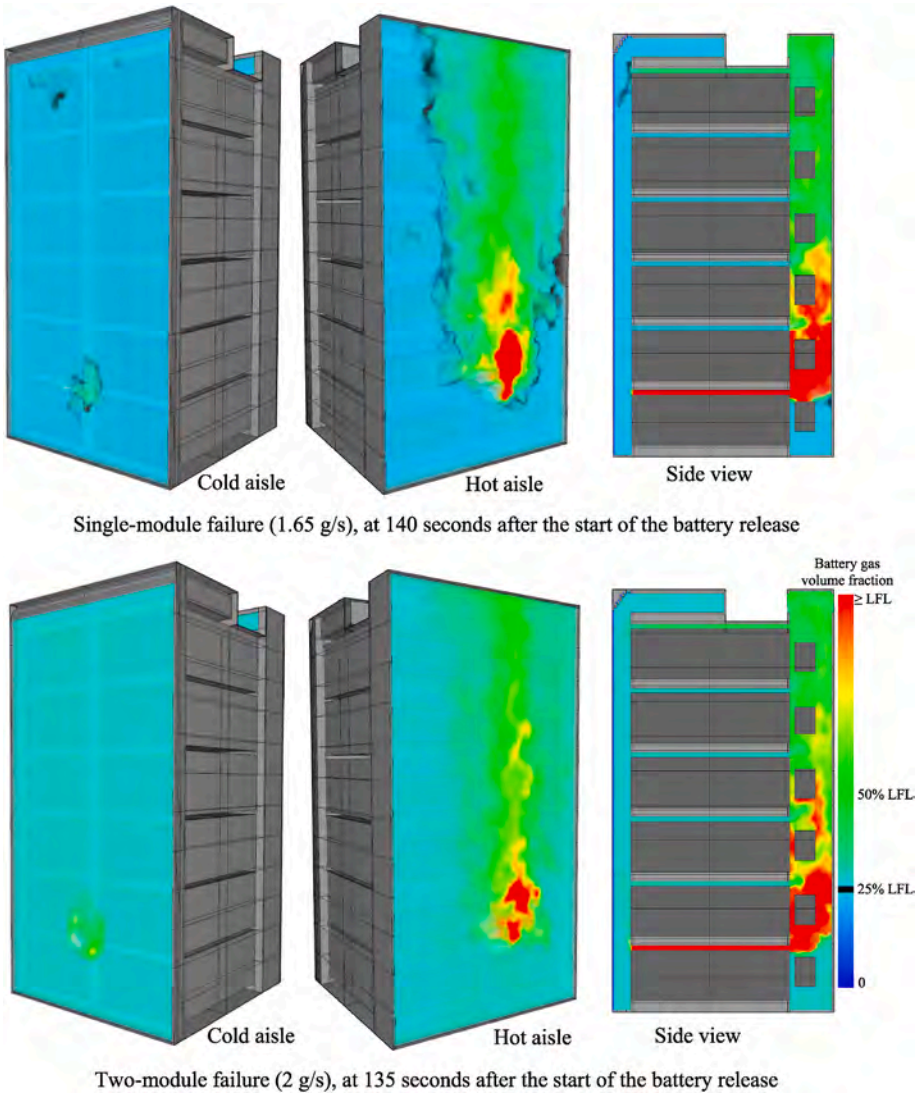

Fig. 15. Battery gas concentration contours during explosion prevention system steady-state operation.

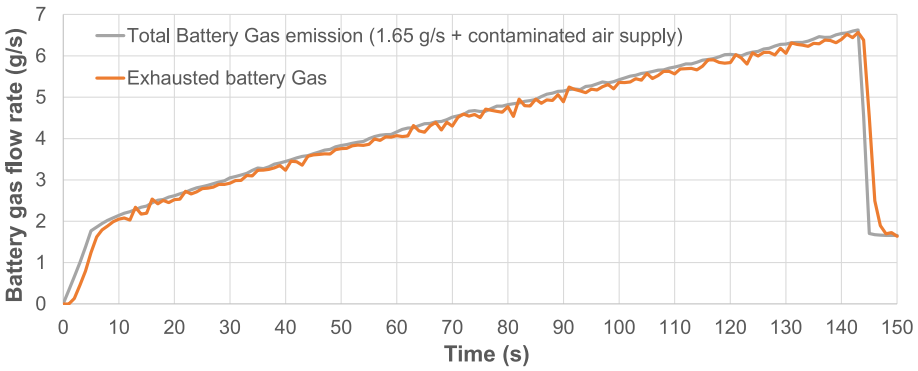

Fig. 16. Evolutions over time of the battery gas sources and release out of the failing half stack for the single-module failure event.

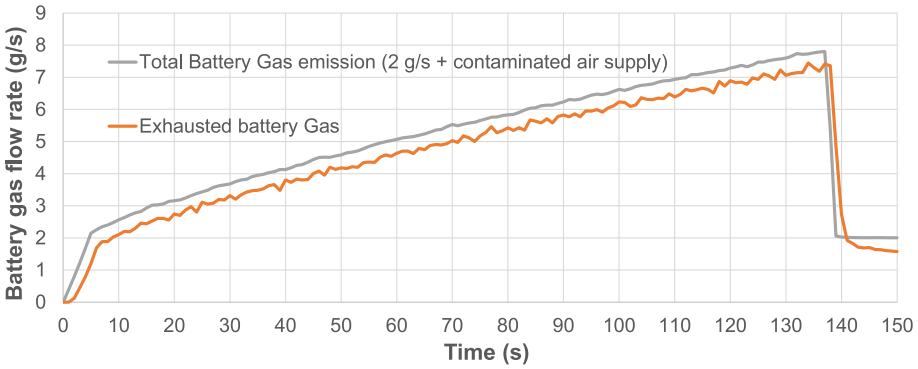

Fig. 17. Evolutions over time of the battery gas sources and release out of the failing half stack for the two-module failure event.

global battery gas volume fraction lower than 25% of its LFL. The explosion prevention system of the Powin Stack™ 360 ESS enclosure utilizes the HVAC system that is switched to its economizer mode (allowing clean air to enter the enclosure and battery gas and air mixture to exit the enclosure) from its recirculating mode.

Two credible failure scenarios based on UL 9540A data were simulated to assess the ventilation system's performance (single- and two-module failure). The analysis was performed at an enclosure level and a stack level using the FDS CFD tool. A gas release model was used as the basis for hazard definition, in accordance with NFPA 855.

The study performed in this work did not consider the activation of a clean agent or an aerosol-based suppression system that may impact the performance of the detection system and the ventilation system. Finally, the explosion prevention system presented here is only limited to the removal of flammable battery gas generated due to the non-flaring decomposition of batteries and is not intended to suppress the growth of an evolving fire or handle a toxic exposure hazard.

The study included two CFD analyses.

- an enclosure-level dispersion analysis to assess the capability of the explosion prevention to maintain the global battery gas volume fraction lower than 25% of its LFL.
- a stack-level dispersion analysis to address the plausibility of developing an explosive environment inside the half stack cabinet while the stack fans operate at 800 CFM (0.38 m^3/s). (In addition, this analysis quantified the influence of battery gas accumulation inside the stack on the container-level analysis.)

The container-level analysis demonstrated the capability of the explosion prevention system to maintain the global battery gas volume fraction inside the container under 25% of its LFL for the two considered failure events. In addition, the analysis assessed the amount of battery gas that would be returning to the failing half stack cabinet while the HVAC system operated in the recirculation mode at the start of the failure events. This estimation was used as an input to the stack-level analysis.

The stack-level analysis was performed to assess the development of an explosive environment inside the half stack cabinet due to the release of battery gas from non-flaring failed battery cells. The half stack itself would cause the released battery gas to accumulate inside the cabinet as it is an enclosed geometry. The stack fans were operating prior to the release of the battery gas in this analysis. This follows the assumption of fans operating if a cell temperature exceeds T_{th}. Note that this is the key assumption for the explosion prevention system to perform successfully.

For the two considered failure events, the internal stack dispersion analysis showed that the peak global volume fraction of the accumulated battery gases inside the stack would be greater than the 25% LFL limit but only for approximately 1 min prior to the activation of the ESS container explosion prevention system. The global battery gas release would reach a steady state of approximately 0.5% vol/vol of air (8% LFL) during the steady-state operation of the explosion prevention system. The explosion prevention system does not prevent local gas concentrations from exceeding the LFL in close proximity to the issuing battery gas or where gases can accumulate. Local spots in the container may have concentrations above the LFL. The evaluated exhaust system significantly reduces the risk of an explosion but does not eliminate an explosion risk.

Overall, the conceptual design assessed in this report meets the intent of NFPA 69 and keeps the global battery gas concentration below 25% of LFL during the steady-state operation for both failure scenarios.

Author contribution statement

Anil Kapahi - Conceptualization, Methodology, Supervision, Writing, review, and editing.Alberto Alvarez-Rodriguez – Formal analysis, Visualization.Sunil Lakshmipathy – Formal analysis, Visualization.

Stefan Kraft - Formal analysis.Jens Conzen- Formal analysis.Angelica Pivarunas – Project Management and Administration.Rody Hardy - Project Management and Administration.Paul Hayes - Project Management and Administration, review.

Declaration of competing interest

The authors declare the following financial interests/personal relationships which may be considered as potential competing interests: Anil Kapahi reports financial support was provided by Jensen Hughes Inc.

Data availability

Data will be made available on request.

References

ANSI/CAN/UL, 2019. UL 9540A: Standard for Test Method for Evaluating Thermal Runaway Fire Propagation in Battery Energy Storage Systems, fourth ed. Underwriters Laboratories Inc.

ASTM E918, 2011. Practice for Determining Limits of Flammability of Chemicals at Elevated Temperature and Pressure. s.l., s.n.

Balakrishnan, P.G., Ramesh, R., Prem Kumar, T., 2006. Safety mechanisms in lithium-ion batteries. J. Power Sources 155, 401–414. April.

Bisschop, R., Willstrand, O., Rosengren, M., 2020. Handling lithium-ion batteries in electric vehicles: preventing and recovering from hazardous events. Fire Technol. 56, 2671–2694. November.

Available at: Blunt, J., Hiller, K., 2021 https://www.wsj.com/articles/.[Online] https://www.wsj.com/articles/battery-storage-soars-on-u-s-electric-grid-11640082783?reflink=desktopwebshare_permalink.

Bravo Diaz, L., et al., 2020. Review—meta-review of fire safety of lithium-ion batteries: industry challenges and Research contributions. J. Electrochem. Soc., January 167, 090559.

Eckhoff, R.K., 2009. Dust explosion prevention and mitigation, status and developments in basic knowledge and in practical application. Int. J. Chem. Eng. 12, 2009(Article ID 569825).

Essl, C., Golubkov, A.W., Fuchs, A., 2020. Comparing different thermal runaway triggers for two automotive lithium-ion battery cell types. J. Electrochem. Soc. 167, 130542. October.

Fernandes, Y., Bry, A., de Persis, S., 2018. Identification and quantification of gases emitted during abuse tests by overcharge of a commercial Li-ion battery. J. Power Sources, June 389, 106–119.

Ghiji, M., Edmonds, S., Moinuddin, K., 2021. A review of experimental and numerical studies of lithium ion battery fires. Appl. Sci., January 11, 1247.

Gully, Ben, Helgesen, Henrik, Skogtvedt, John Erik, Kostopoulos, Dimitrios, Mjøs, Narve, Huser, Asmund, Frithiof, Nathaniel, , Gerd Petra Haugom, Sverud, Terje, 2019. Technical Reference for Li-Ion Battery Explosion Risk and Fire Suppression. s.l., s.n.

Long, D., 2022 ([Online]). https://storagewiki.epri.com/index.php/BESS_Failure_Event_Database.

Mxarvair, n.d. Wall Mount Air Conditioner Product Data Sheet, Models MAA1020A-Maa1060a & MGA1072A, *revision 4*. s.l.:s.n.

McGrattan, K., et al., 2020. Fire Dynamics Simulator, User's Guide. August 21. In: NIST Special Publication 1019, Sixth Edition (FDS Version 6.7.5). National Institute of Standards and Technology, Gaithersburg, Maryland, USA *(and VTT Technical Research Centre of Finland*, Espoo, Finland, s.l.: s.n).

NFPA, 2018. *NFPA 68: Standard On Explosion Protection by Deflagration Venting.* 2018 Ed. s.L. National Fire Protection Association.

NFPA, 2019. In: NFPA 69: Standard on Explosion Prevention Systems. National Fire Protection Association, 2019.

NFPA, 2020. *NFPA 855 Standard For the Installation Of Stationary Energy Storage Systems.* s.L. National Fire Protection Association.

Roth, E.P., Doughty, D.H., Pile, D.L., 2007. Effects of separator breakdown on abuse response of 18650 Li-ion cells. J. Power Sources 174, 579–583. December.

Shen, R., et al., 2020. Recent application of Computational Fluid Dynamics (CFD) in process safety and loss prevention: a review. J. Loss Prev. Process. Ind. 67, 104252.

U.S. Energy Information Administration, 2021. Battery Storage in the United States: an Update on Market Trends (s.l.: s.n).

Zalosh, R., Gandhi, P., Barowy, A., 2021. Lithium-ion energy storage battery explosion incidents. J. Loss Prev. Process. Ind. 72, 104560.